ETH_zürich_

Global Ionospheric Modeling Using Multi-GNSS: A Machine Learning Approach

Conference Paper

Author(s):
Mao, Shuyin; Kłopotek, Grzegorz; Pan, Yuanxin (iD); Soja, Benedikt (iD)

GLOBAL IONOSPHERIC MODELING USING MULTI-GNSS: A MACHINE LEARNING APPROACH

Shuyin Mao, Grzegorz Kłopotek, Yuanxin Pan, Benedikt Soja

ETH Zurich
Institute of Geodesy and Photogrammetry
8093 Zurich, Switzerland

ABSTRACT

The ionosphere is a significant error source in space-geodetic techniques, such as the Global Navigation Satellite System (GNSS) and satellite radar altimetry. This is especially pronounced for single-frequency receivers, as ionospheric delays cannot be mitigated by ionosphere-free combinations. Therefore, for high-precision space applications, we need an accurate ionospheric model to provide ionospheric corrections at desired times and locations, such as global ionospheric maps (GIMs) that depict the global distribution of vertical total electron content (VTEC). In this study, we propose a neural network (NN)-based global ionospheric model to predict global VTEC with higher accuracy compared with conventional GIMs. We first determined VTEC based on the carrier-to-code leveling method using multi-GNSS observations from global IGS stations. The derived VTEC time series for all training station-satellite pairs were then used to train the NN-based model. During our experiment in April 2022, a period of high solar activity, the average mean absolute error of VTEC predictions at 47 global test stations was 1.7 TECU. The performance of the NN-based models were also evaluated by single-frequency precise point positioning and compared with GIMs provided by the Chinese Academy of Sciences since the same differential code bias products were used. The NN-based models demonstrated a noteworthy enhancement in the positioning precision at 47 test stations, achieving improvements of 12%, 20%, and 8% for the east, north, and up components, respectively.

Index Terms— Ionosphere, machine learning, GNSS, neural network

1. INTRODUCTION

The ionosphere is the ionized part of the Earth's upper atmosphere, characterized by a significant concentration of ions and free electrons. These electrons significantly affect the propagation of radio waves, causing signal delays and reducing the reliability of radio communication and navigation systems. For instance, Global Navigation Satellite Systems (GNSS) can experience signal delays of many tens of meters due to the ionosphere under solar maximum conditions or solar storms, introducing large errors in positioning [1]. To address these errors, precise ionospheric modeling becomes essential, which enables us to predict and compensate for ionospheric delays, ensuring more accurate and reliable GNSS applications.

Global ionospheric maps (GIMs) from the International GNSS Service (IGS) and its Ionosphere Associate Analysis Centers (IAACs) are widely used products to correct ionospheric delays in GNSS signals, especially for single-frequency applications where ionospheric delays cannot be mitigated with the ionosphere-free combination of observations. GIMs depict the global distribution of vertical total electron content (VTEC), presented in the IONosphere Map EXchange Format (IONEX) for the convenience of the interested parties. With a typical spatial resolution of $5°$ in longitude and $2.5°$ in latitude, GIMs can achieve an overall accuracy of approx. 2-8 TEC Units (TECU) [2]. To generate GIMs, traditional mathematical methods, such as spherical harmonics, B-splines, and Kriging interpolation, are commonly used. Although these techniques can sufficiently capture large-scale and global features of the ionosphere, they tend to smooth out local variations and irregularities due to the limited spatial resolution typically chosen by the providers.

Machine learning (ML) methods offer new solutions for addressing these challenges. As an effective tool to uncover the nonlinear connections between inputs and outputs, ML can be used to model relationships between ionospheric variations and parameters like time and location, as well as solar and geomagnetic indices. In recent years, various ML algorithms have been increasingly employed in ionospheric modeling and show great potential [3, 4, 5]. However, these studies focused mostly on temporal ionospheric modeling, while the spatial modeling of the ionosphere was rarely discussed, especially at a global scale.

In this study, we propose a neural network-based (NN-based) method for global VTEC modeling as an alternative to conventional GIMs. The goal is to improve the accuracy of ionospheric models. In the following sections, we first intro-

duce the methodology of GNSS VTEC estimation and ML-based global VTEC modeling. Then, the data and experiment settings are described. Finally, the performance of the generated NN-based global ionospheric model is discussed.

2. METHODOLOGY

2.1. GNSS VTEC estimation

We used the carrier-to-code leveling (CCL) method to estimate VTEC based on multi-GNSS observations [6]. The obtained VTEC time series were then used as target features to train the NN-based model.

To derive TEC from GNSS measurements, the geometry-free combination is widely used due to the frequency-dependent characteristics of ionospheric delay, which can be written as follows:

$$P_{r,GF}^s = k(\frac{1}{f_1^2} - \frac{1}{f_2^2})STEC_r^s + DCB_r - DCB^s + e_{r,GF}^s$$

$$L_{r,GF}^s = -k(\frac{1}{f_1^2} - \frac{1}{f_2^2})STEC_r^s + B_{r,GF}^s + \epsilon_{r,GF}^s,$$

$$(1)$$

where k is a constant value of 40.3 m^3s^{-2}; f_1 and f_2 represent the frequencies of GNSS signals (GPS: $L1$ and $L2$, Galileo: $E1$ and $E5a$); $STEC_r^s$ denotes the slant total electron content (STEC) along the satellite-receiver path; DCB_r and DCB^s represent the differential code biases (DCB) related to the receiver and satellite, which can be corrected by DCB products; $B_{r,GF}^s$ is the geometry-free ambiguity contaminated by carrier-phase hardware delays, which needs to be set up for each new satellite arc and whenever a cycle slip occurs; $e_{r,GF}^s$ and $\epsilon_{r,GF}^s$ represent the observation noise and unmodeled errors like multipath.

Based on Equation 1, we can estimate the phase ambiguity and STEC simultaneously. Finally, STEC values are transformed into VTEC values at each ionospheric pierce point (IPP) using the single-layer model (SLM) mapping function:

$$VTEC_r^s = \sqrt{1 - \left(\frac{R_e}{R_e + H_{ion}} \cos\theta\right)^2} STEC_r^s \quad (2)$$

where R_e represents the radius of the Earth; H_{ion} represents the height of the ionospheric layer and is set to 450 km in this study; and θ is the elevation angle of the satellite.

2.2. ML-based global VTEC modeling

We used a feed-forward NN to model the VTEC on a global scale using available GNSS observations from IGS stations. The NN has three key layers: the input layer, the hidden layer(s), and the output layer. After hyperparameter tuning, we used three hidden layers, each with 60 neurons. As shown in Fig. 1, seven input features, including location and time information, were used. Note that we used solar magnetic (SM)

latitude (SM_LAT) and longitude (SM_LON), instead of geographic coordinates, to take into account the impact of solar radiation and geomagnetic activities. We used sine and cosine terms of SM longitude to ensure the continuity of the model at $-180°$ and $180°$. Besides, sine and cosine components of seconds of day (SODS and SODC) and day of year (DOYS and DOYC) were incorporated as temporal features.
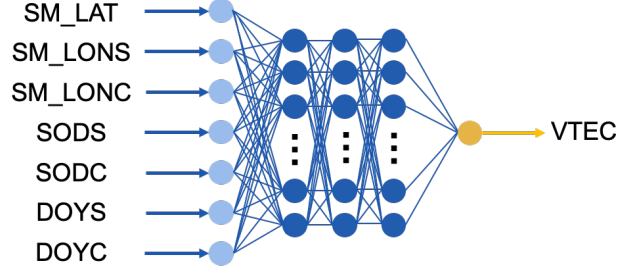

Fig. 1. Neural network model, input features, and the target feature utilized in this study.

3. DATA AND EXPERIMENT

In this study, we used GPS and Galileo observations from approx. 300 IGS stations distributed globally. The data were processed with a 30-second sampling resolution based on the CCL method implemented in CamaliotGNSS [7]. The latter employs a Kalman filter (KF) with a smoother to derive VTEC time series for each station-satellite pair. As an input to the KF-based CCL approach, satellite and receiver DCB products [8] from the Chinese Academy of Sciences (CAS) were used to correct the geometry-free observables, as shown in Equation 1. An elevation cut-off angle of $35°$ was used during the preprocessing of machine learning to exclude VTEC estimates with low accuracy since they were greatly affected by errors in the SLM mapping function. The experiment covered the period from April 1st to 30th, 2022. Fig. 2 displays the time series of F10.7 and the Disturbance Storm-Time (Dst) index during the period. F10.7 is represented in red, which can be considered an indicator of solar activity, while the Dst is in blue, serving as a proxy for geomagnetic activity. Notably, the F10.7 index reflects high solar activity in April 2022, with its value ranging from 96 solar flux units (sfu) to 147 sfu. As illustrated by the Dst index, there was a geomagnetic storm on April 14th, where the Dst index dropped to -80 nT at 21:00. By selecting this experiment period, we can better evaluate the performance of the proposed model during an active ionosphere period.

We trained the neural network (NN) model daily, utilizing VTEC time series with a 30-second resolution. This approach ensures comparability with conventional GIMs, which are also updated daily. As a result, 30 daily NN-based models were generated. We selected 47 globally distributed IGS sta-
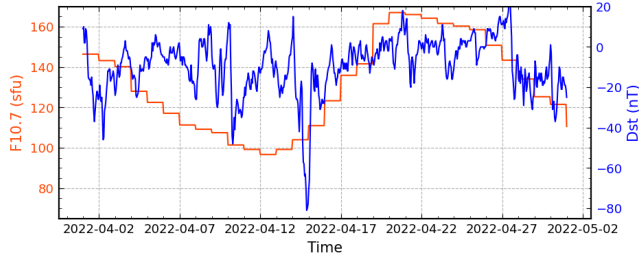
Fig. 2. Time series of F10.7 solar flux index (red) and the Disturbance Storm-Time (Dst) index (blue) in April 2022.
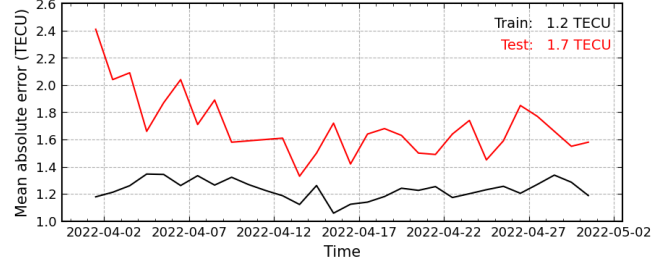
tions as our test stations. The remaining stations were used as training data. Fig. 3 displays the distribution of training and test stations on April 4th, 2022. To evaluate the performance of our NN-based model, single-frequency precise point positioning (SF-PPP) tests were conducted on the test stations. The positioning accuracy of NN-based models was compared with that of traditional GIMs from CAS since the same DCB products were used to produce VTEC time series in our case. Note that the CAS GIMs are based on the traditional spherical harmonics and generalized trigonometric series method [9]. For a fair comparison, the 47 test stations selected above were not utilized to generate the CAS GIMs either.
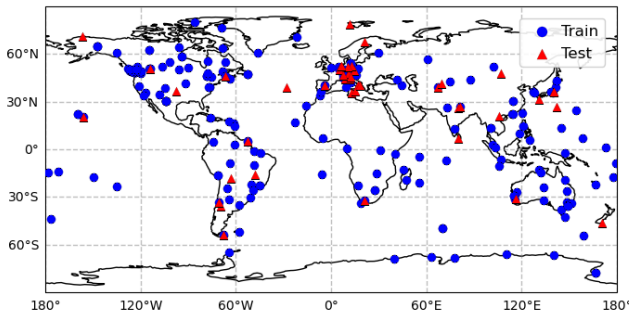
Fig. 3. Distribution of training and test stations on April 4th, 2022. Blue dots and red triangles represent the training and test stations, respectively.

4. RESULTS

Fig. 4 shows the time series of mean absolute error (MAE) of the NN-based VTEC predictions compared to CCL VTEC. The black line represents the MAE at all training stations, while the red line represents the MAE at test stations. Concerning the experiment period, the average training MAE and test MAE are 1.2 TECU and 1.7 TECU, respectively. Compared with the training MAE, the test MAE shows larger variations, ranging from a minimum of 1.3 TECU to a maximum of 2.4 TECU. For the geomagnetic storm day (April 14th), the test MAE increases to 1.5 TECU compared to 1.3 TECU

on April 13th, a geomagnetic quiet day with Dst higher than -30 nT.

The station-specific MAE is shown in Fig. 5. There is a clear correlation between MAE and stations' latitudes, which is expected considering the VTEC magnitude distribution. Specifically, for low-latitude stations, prediction errors tend to be higher than those for stations located at mid- and high-latitudes, reaching a maximum MAE of approx. 6 TECU. Conversely, for mid-latitude stations, the prediction errors are usually within 2 TECU.

Fig. 4. Time series of daily mean absolute error between NN-based VTEC and CCL VTEC at training and test stations.
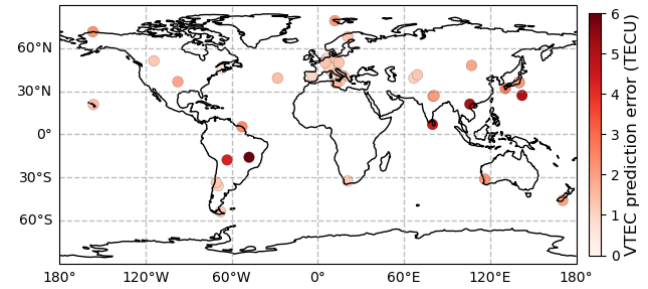
Fig. 5. VTEC prediction error (mean absolute error between NN-based VTEC and CCL VTEC) at test stations.

We also conducted SF-PPP tests to evaluate the positioning performance when utilizing our NN-based models. Observations on GPS L1 and Galileo E1 frequencies were used. The ionospheric delays in L1/E1 signals were directly corrected with the predictions from the NN-based models. Satellite orbit and clock errors were computed with the final products from the Center for Orbit Determination in Europe (CODE) [10]. The station coordinates were estimated in kinematic mode. The same SF-PPP test was also conducted with CAS GIMs and the results were compared to those using our NN models.

Fig. 6 displays the 3D positioning error of SF-PPP using the NN-based models at each test station. Notably, lower positioning errors (approx. 0.5 m) are observed at mid-latitude stations, while errors at low-latitude stations are relatively larger, ranging from 1.6 m to 3.6 m. The average positioning errors are shown in Table 1. Overall, the NN-based models can achieve an accuracy of 0.37, 0.37, and 0.78 m for the

Table 1. Average positioning error at 47 test stations over the experiment period of NN-based models and CAS GIMs

	NN-model	CAS-GIM	Improvement
East (m)	0.37	0.42	12%
North (m)	0.37	0.46	20%
Up (m)	0.78	0.85	8%
3D (m)	0.95	1.07	11%

east, north, and up components during the experiment period. Compared with CAS GIMs, the positioning accuracy is visibly enhanced by using the NN-based models, with an improvement of 12%, 20%, and 8% for the east, north, and up position components, respectively. The improvements do not show a clear dependence on latitude.
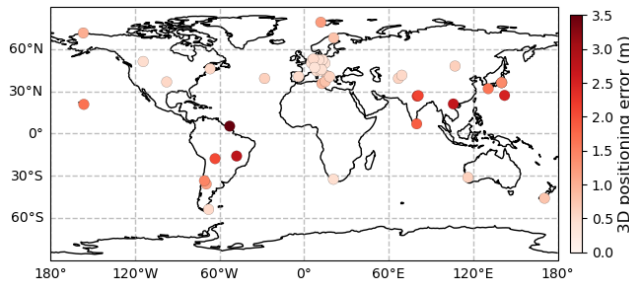
Fig. 6. 3D positioning error based on the SF-PPP processing at test stations using the NN-based VTEC model.

5. CONCLUSIONS

In this study, we proposed daily NN-based ionospheric models for global VTEC prediction. The models were trained based on daily VTEC time series and achieved an average MAE of 1.7 TECU at global test stations during a period of high solar activity. The generated models can be used to predict ionospheric corrections globally. Based on the conducted SF-PPP tests, the NN-based models tend to provide more accurate ionospheric corrections than traditional GIMs from CAS, with distinct improvements in positioning precision. These results demonstrate the great potential of utilizing ML methods in global ionospheric modeling, which can efficiently improve the accuracy of ionospheric predictions compared with traditional mathematical methods. Considering that the IONEX is a widely employed standard for the exchange of ionospheric products, we plan to generate NN-based GIMs formatted in IONEX in the future, providing user-friendly products for the interested research communities.

6. REFERENCES

[1] P. K. Enge, "The Global Positioning System: Signals, measurements, and performance," *International Journal of Wireless Information Networks*, vol. 1, pp. 83–105, 1994.

[2] D. Roma-Dollase, M. Hernández-Pajares, A. Krankowski, K. Kotulak, R. Ghoddousi-Fard, Y. Yuan, Z. Li, H. Zhang, C. Shi, C. Wang, et al., "Consistency of seven different GNSS global ionospheric mapping techniques during one solar cycle," *Journal of Geodesy*, vol. 92, pp. 691–706, 2018.

[3] X. Ren, P. Yang, H. Liu, J. Chen, and W. Liu, "Deep Learning for Global Ionospheric TEC Forecasting: Different Approaches and Validation," *Space Weather*, vol. 20, no. 5, 2022.

[4] D. Yang, H. Fang, and Z. Liu, "Completion of Global Ionospheric TEC Maps Using a Deep Learning Approach," *Journal of Geophysical Research: Space Physics*, vol. 127, no. 5, pp. e2022JA030326, 2022.

[5] R. Natras, A. Goss, D. Halilovic, N. Magnet, M. Mulic, M. Schmidt, and R. Weber, "Regional Ionosphere Delay Models Based on CORS Data and Machine Learning," *NAVIGATION: Journal of the Institute of Navigation*, vol. 70, no. 3, 2023.

[6] L. Ciraolo, F. Azpilicueta, C. Brunini, A. Meza, and S. M. Radicella, "Calibration errors on experimental slant total electron content (TEC) determined with GPS," *Journal of geodesy*, vol. 81, pp. 111–120, 2007.

[7] G. Kłopotek, Y. Pan, T. Sturn, R. Weinacker, L. See, L. Crocetti, M. Awadaljeed, M. Rothacher, I. McCallum, S. Fritz, et al., "A Cloud-native Approach for Processing of Crowdsourced GNSS Observations and Machine Learning at Scale: A Case Study from the CAMALIOT Project," *Advances in Space Research*, 2024.

[8] N. Wang, Y. Yuan, Z. Li, O. Montenbruck, and B. Tan, "Determination of differential code biases with multi-GNSS observations," *Journal of Geodesy*, vol. 90, pp. 209–228, 2016.

[9] Z. Li, N. Wang, A. Liu, Y. Yuan, L. Wang, M. Hernández-Pajares, A. Krankowski, and H. Yuan, "Status of CAS global ionospheric maps after the maximum of solar cycle 24," *Satellite Navigation*, vol. 2, no. 1, pp. 1–15, 2021.

[10] S. Schaer, A. Villiger, D. Arnold, R. Dach, L. Prange, and A. Jäggi, "The CODE ambiguity-fixed clock and phase bias analysis products: generation, properties, and performancec," *Journal of Geodesy*, vol. 95, pp. 1–25, 2021.